Hybrid RANS/LES of plane jets impinging on a flat plate at small nozzle-plate distances

S. KUBACKI[1], J. ROKICKI[1], E. DICK[2], J. DEGROOTE[2], J. VIERENDEELS[2]
[1]*Institute of Aeronautics and Applied Mechanics, Warsaw University of Technology, Nowowiejska 24, 00-665, Warsaw, Poland;*
[2]*Department of Flow, Heat and Combustion Mechanics, Ghent University, St.–Pietersnieuwstraat 41, B-9000, Ghent, Belgium.*

e-mail: slawomir.kubacki@meil.pw.edu.pl

Abstract

A k-ω based hybrid RANS/LES (Reynolds Averaged Navier Stokes/Large Eddy Simulation) model is tested for simulation of plane impinging jets at various nozzle-plate distances (H/B, where H is the distance and B is the slot width) and various Reynolds numbers (based on the slot width and the velocity in the symmetry plane). The studied combinations are H/B=2 for Re=10000, H/B=4 for Re=18000 and H/B=9.2 for Re=20000. The focus is on small distance of the nozzle exit to the plate. In LES mode, the hybrid RANS/LES model uses two definitions of the local grid size, one based on the maximum distance between the cell faces in the destruction term of the turbulent kinetic energy equation and one based on the cube root of the cell volume in the eddy-viscosity formula. This allows accounting for flow inhomogeneity on anisotropic grids. In RANS mode, the hybrid model turns into the newest version of the k-ω model by Wilcox.

Key words: plane impinging jet, turbulence modelling, hybrid RANS/LES model, Large Eddy Simulation

1. Introduction

Plane impinging jets were studied experimentally [1-8] and numerically using LES [9-11] in order to provide a database for assessment of the qualities of turbulence models, to study the influence of the inlet conditions on the impingement plate shear stress and heat transfer distributions and to understand the relationship between heat transfer and shear stress along the plate. DNS were performed [11, 12] to clarify the effect of the inlet disturbances on the flow and heat transfer characteristics along the impingement plate or to study the effect of nozzle-plate distance on the location of the secondary peak in the shear stress and the heat transfer profiles. The predictive qualities of various RANS models were verified by Fernandez et al. [13] and Jaramillo et al. [14], among others, for plane impinging jets at various nozzle-plate distances and Reynolds numbers. For large nozzle-plate distance, RANS models suffer from difficulties in reproducing the turbulence mixing in the developing shear layers of the jet as well as in capturing the correct level of shear stress and heat transfer in the impact zone. This poses a difficulty in application of the RANS-based techniques in analysis of complex flow systems in which free jet development and its subsequent impingement largely determine the level of the wall shear stress and local heat transfer rate along the impingement wall. For small nozzle-plate distance, where the flow in the impact zone physically is laminar, the prediction of the shear stress and heat transfer levels in the impact zone are basically correct with RANS models due to use of stress limiters which damp most

of the turbulence in the impact zone. The transition from laminar to turbulent state in the developing boundary layer on the plate is completely ignored by RANS models.

In the present work, a k-ω based hybrid RANS/LES model and the k-ω RANS model of Wilcox [15] are employed to study their applicability in reproducing the plane impinging jet flow characteristics at low nozzle-plate distances (H/B=2 and 4) and at various Reynolds numbers (10000 and 18000). This means for impact of the jet onto the plate before complete mixing of the shear layers. The centre of the impact zone is then in laminar state and the developing boundary layer on the plate undergoes transition to turbulent state. The transitional flow cannot be correctly simulated with the RANS turbulence model, but we will demonstrate that the hybrid model is basically correct. The test case with the large nozzle-to-plate distance (H/B=9.2, Re=20000) is only meant to demonstrate the correct setting of the inflow conditions. The reliability of the hybrid model will be demonstrated by comparing results of mean velocity profiles, profiles of fluctuating velocity components and skin friction on the plate with results from LES using a dynamic Smagorinsky model and experiments.

The hybrid RANS/LES model analysed here belongs to the class of unified DES-type approaches, as first proposed by Strelets [16]. For a classification of hybrid approaches, we refer to Fröhlich and von Terzi [17]. The local grid size, replacing the turbulent length scale in the LES mode of the hybrid model, is introduced in both the destruction term of the turbulent kinetic energy equation and in the eddy-viscosity formula, according to methods first proposed by Davidson and Peng [18], Kok et al. [19] and Yan et al. [20]. In RANS mode, the newest version of the k-ω model of Wilcox [15] is recovered. Two definitions of the local grid size are used to better account for flow inhomogeneity on anisotropic grids. The model was already tested on round impinging jets [21]. A simpler version was tested on plane impinging jets at large nozzle-plate distances by Kubacki and Dick [22] and Kubacki et al. [23].

2. The hybrid RANS/LES model

The transport equations for the turbulent kinetic energy, k, and the inverse of the turbulent time scale (frequency), ω, read:

$$\frac{\partial k}{\partial t}+\frac{\partial (U_j k)}{\partial x_j}=\tau_{ij}\frac{\partial U_i}{\partial x_j}-\max\left(\beta^* k\omega,\frac{k^{3/2}}{C_{DES}\Delta}\right)+\frac{\partial}{\partial x_j}\left[\left(\nu+\sigma^*\frac{k}{\omega}\right)\frac{\partial k}{\partial x_j}\right], \tag{2.1}$$

$$\frac{\partial \omega}{\partial t}+\frac{\partial (U_j \omega)}{\partial x_j}=\alpha\frac{\omega}{k}\tau_{ij}\frac{\partial U_i}{\partial x_j}-\beta\omega^2+\frac{\sigma_d}{\omega}\frac{\partial k}{\partial x_j}\frac{\partial \omega}{\partial x_j}+\frac{\partial}{\partial x_j}\left[\left(\nu+\sigma\frac{k}{\omega}\right)\frac{\partial \omega}{\partial x_j}\right]. \tag{2.2}$$

In these equations, ν is the kinematic molecular viscosity, and the modelled stress tensor and the shear rate tensor are $\tau_{ij}=2\nu_t S_{ij}-2/3k\delta_{ij}$ and $S_{ij}=1/2(\partial U_i/\partial x_j+\partial U_j/\partial x_i)-1/3(\partial U_k/\partial x_k)\delta_{ij}$, respectively. The local grid size Δ is defined by $\Delta=\max(\Delta_x, \Delta_y, \Delta_z)$ where Δ_x, Δ_y, Δ_z denote the distances between the cell faces in x, y and z directions. The grid size is multiplied with a tuning constant C_{DES}, which we derive later. The basic model is the k-ω RANS of Wilcox [15]. The motivation for the modification of the destruction term in (2.1) is that the dissipation in the k-ω RANS model is $\varepsilon=\beta^* k\omega=k^{3/2}/L_t$, where the turbulent length scale is $L_t=k^{1/2}/(\beta^*\omega)$. So, it means that in the dissipation term, the turbulent length scale is replaced by the grid size when the model transfers to LES mode. The choice of the grid size measure is crucial in any LES like formulation [17, 24, 25]. The literature shows that there is a preference for the maximum size in a DES (Detached Eddy Simulation) formulation [20, 25], while there is a preference for the cube root measure in an LES formulation [17, 24]. For the length scale in the k-equation (2.1), we take the maximum size, as by the substitution of the length scale, a Detached Eddy Simulation (DES) model is obtained, in the style as first proposed by Strelets [16].

The closure coefficients are [15]:

$$\beta^* = 0.09, \quad \alpha = 0.52, \quad \beta = \beta_0 f_\beta, \quad \beta_0 = 0.0708,$$
$$\sigma = 0.5, \quad \sigma^* = 0.6, \quad \sigma_{do} = 0.125,$$
$$f_\beta = \frac{1+85\chi_\omega}{1+100\chi_\omega}, \quad \chi_\omega = \left|\frac{\Omega_{ij}\Omega_{jk}S_{ki}}{(\beta^*\omega)^3}\right|, \quad \sigma_d = \begin{cases} 0 & \text{for} \quad \dfrac{\partial k}{\partial x_j}\dfrac{\partial \omega}{\partial x_j} \le 0 \\ \sigma_{do} & \text{for} \quad \dfrac{\partial k}{\partial x_j}\dfrac{\partial \omega}{\partial x_j} > 0 \end{cases}$$

where $\Omega_{ij}=1/2(\partial U_i/\partial x_j-\partial U_j/\partial x_i)$ is the vorticity tensor.

The eddy-visosity is defined according to Davidson and Peng [18] and Kok et al. [19] by

$$\nu_t = \min\left(\frac{k}{\omega}, \beta^* C_{DES}\sqrt{k}\Delta_{LES}\right), \tag{2.3}$$

where $\Delta_{LES}=(\Delta_x\Delta_y\Delta_z)^{1/3}$. The motivation for this modification is that the RANS eddy viscosity is $\nu_t=\beta^* L_t k^{1/2}$. So, it means that also in the eddy viscosity expression, the turbulent length scale is replaced by the grid size. The chosen grid size is here the cube root measure, so the typical LES grid size. The grid size is multiplied with the tuning constant C_{DES}. The justification for using different grid scales in Eq. (2.3) and in the k-equation (Eq. 2.1) is that, under local equilibrium (production of k equal to dissipation of k), the eddy viscosity reduces in LES mode to a Smagorinsky subgrid viscosity

$$\nu_t = \left(C_s\Delta_{LES}\left(\frac{\Delta}{\Delta_{LES}}\right)^{1/4}\right)^2 S. \tag{2.4}$$

with $C_s=(\beta^*)^{3/4}C_{DES}$ set to the usual value 0.1, which gives $C_{DES}=0.6086$ and with the magnitude of the shear rate $S=(2S_{ij}S_{ij})^{1/2}$. The role of the term $(\Delta/\Delta_{LES})^{1/4}$ is to increase the eddy viscosity on high aspect ratio cells, with respect to the value obtained by the cube root grid size in all turbulence length scale substitutions. We follow here the approach by Scotti et al. [24], who proved much better predictive qualities of LES on anisotropic grids by an increased eddy viscosity.

For the RANS simulations [15], a stress limiter is applied. This means that the turbulent viscosity ν_t is defined by

$$\nu_t = \frac{k}{\tilde{\omega}}, \quad \tilde{\omega} = \max\left(\omega, C_{lim}\sqrt{\frac{2S_{ij}S_{ij}}{\beta^*}}\right) \tag{2.5}$$

with $C_{lim}=7/8$. The RANS stress limiter [15] is omitted in Eq. (2.3) in the hybrid RANS/LES model. Tests showed that the stress limiter has only negligible effect on the results of impinging jet flows with the hybrid RANS/LES model. The limiter is only significant for the RANS model.

As boundary conditions, k=0 at walls and $\omega = u_\tau^2 S_R / \nu$ in the centre of a cell at a wall, with $u_\tau=(\tau_w/\rho)^{1/2}$, $\tau_w=\mu\cdot S$, $S_R = \min[(200/k_s^+)^2, 6/(\beta_0(\Delta y^+)^2)]$, where $\Delta y^+=\Delta y\cdot u_\tau/\nu$, k_s^+ is a dimensionless roughness height, Δy is the distance to the wall of the centre of the cell, ρ is the fluid density and μ is the dynamic molecular viscosity. Since the wall is assumed to be hydraulically smooth, the dimensionless roughness height was set to $k_s^+ = 4$, according to Wilcox [15].

One has to note that the main difference between the newest version of the k-ω model by Wilcox [15] (employed here) and the previous model version [26] is the addition of the cross-diffusion term in the ω-equation (third term on r.h.s. of Eq. 2.2) which limits a spurious sensitivity of the k-ω model to the turbulence quantities specified in the free stream. The other

difference is the addition of the stress-limiter in the eddy-viscosity formula (Eq. 2.5) which limits overprediction of the turbulent shear stress in the stagnation flow regions.

3. Computational framework

The computational domain consists of a rectangular box as shown in Fig 1. Details related to the size of the computational domain, coordinate system, boundary conditions and the number of grid points are given in Table 1. The velocity vector is defined by **U**=U**i** + V**j** +W**k** where the unit vectors **i**, **j** and **k** are aligned with the **x**, **y**, and **z** vectors shown in Fig. 1.

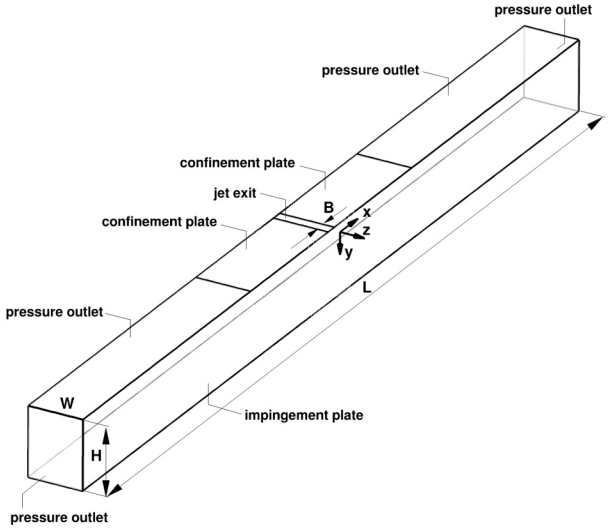

Figure 1. Sketch of computational domain, coordinate system and boundary conditions for plane impinging jet simulation at H/B=4. Periodic conditions are imposed in the z direction.

At the inlet to the computational domain (jet exit) an almost flat mean velocity profile was specified by

$$V(x,0,z) = V_0(1-(2x/B)^{14}), \tag{3.1}$$

where V_0 denotes the mean velocity in the symmetry plane. We show later that the mean velocity profile given by Eq. (3.1) corresponds well with experimental data immediately downstream of the slot. For all cases in Table 1, the turbulence intensity at the jet exit was set to Tu=0.9% in accordance with the experiments of Zhe and Modi [4]. A similar value of the inlet turbulence intensity, 1%, was used by Ashforth-Frost et al. [3]. We use also the measurements by Ashforth-Frost et al. [3] for comparison with our numerical results (the experimental set-up by Ashforth-Frost et al. [3], is very similar to the experimental set-up by Zhe and Modi [4].

The integral length scale was not measured in the inlet plane by Zhe and Modi [4] and Ashforth-Frost et al. [3]. In the present RANS computations, constant values of k and ω were specified at the inlet of the computational domain with Tu=0.9%, while the turbulent (integral) length scale L_t was specified according to Jaramillo et al. [14], namely L_t=0.1667B. Uniform inlet profiles of the turbulent quantities are specified by $k=1.5(Tu\cdot V_0)^2$ and $\omega=k^{1/2}/(\beta^* L_t)$. For the hybrid simulations, the vortex method of Fluent was used to generate the resolved fluctuations in the inlet plane [27]. For the LES, random fluctuations were generated in the inlet plane. The full RANS profiles of k and ω were imposed at the jet exit to reproduce the resolved perturbations. With the vortex method, structures smaller than the grid size are not generated. So, the modelled part of the total fluctuating velocity is automatically not taken into account. The modelled k_{SGS} and ω_{SGS} are prescribed by

$k_{SGS}=(C_{DES}\Delta)^{2/3}\varepsilon^{2/3}=(\beta^{*}k\omega C_{DES}\Delta)^{2/3}$, $\omega_{SGS}=\varepsilon/(\beta^{*}k_{SGS})=\omega k/k_{SGS}$ [21]. This means that the length $C_{DES}\Delta$ is used as representative length scale for the subgrid turbulence. The top boundary, at the height of the jet exit, was split into two parts. A confinement wall was specified for a part of the boundary extending from the slot edges up to the streamwise distance x/B= ±13 [4]. A pressure outlet boundary condition was applied for the remaining part of the top boundary as well as in the outflow planes located at x/B= ±40. This means that relative static pressure was prescribed (set here to zero), as well as the direction of the backflow (which is determined based on the flow direction in the cells adjacent to the boundary) and the values of the transported scalars. In the RANS model simulations the direction of the backflow was simply set to be normal to the pressure outlet boundary. With the pressure outlet condition imposed, a very low value of the turbulent/subgrid to molecular viscosity ratio was prescribed in the computations using the hybrid and LES models in the flow regions re-entering the computational domain (set here to 0.01) while the backflow turbulent length scale was set to L_t=0.1667B. In RANS computations the ratio of the turbulent to molecular viscosity was set to 5 and the turbulent length scale was set to L_t=0.1667B. No fluctuations were generated with the vortex method at the pressure outlet boundaries with the LES and hybrid RANS/LES models. Periodic boundary conditions have been applied in the spanwise *z*-direction.

Table 1
Length *L*, height *H* and width *W* of the computational domains for simulations performed with the hybrid RANS/LES and LES models and the number of cells N_x, N_y, N_z in x, y and z directions.

Case	L/B	H/B	W/B	N_x	N_y	N_z	N_{tot} (M)
H/B=9.2, Re=20000	80	9.2	π	320	320	70	7.2
H/B=4, Re=18000	80	4	π	320	180	70	4.0
H/B=2, Re=10000 (basic)	80	2	π	320	110	70	2.5
H/B=2, Re=10000 (fine)	80	2	π	540	200	140	15.1

The computations using the RANS and the hybrid RANS/LES models have been performed with the Fluent code ver. 12, while the LES simulations have been performed with OpenFOAM. In Fluent, the transport equations (Eqs. 2.1-2.2) were implemented with the user-defined scalar functionality. For the hybrid RANS/LES, a TVD-bounded central scheme was applied to the convective terms in the momentum equations, while for LES it was the central differencing scheme with filtering of high-frequency ripples. The second order upwind scheme was used to the convective terms in the k- and ω-equations (hybrid RANS/LES). For RANS, the second order upwind scheme was used for discretisation of the convective terms in all equations. For temporal discretisation (hybrid RANS/LES and LES), a second-order implicit scheme was applied. An implicit time stepping technique was chosen to guarantee stability for large CFL number. The time step was, however, chosen small enough so that the CFL-number in LES zones was at maximum 2, so that the dissipation due to the time stepping remained small. At each time step, inner iteration steps were applied to lower the residuals for the momentum and the transport equations below 10^{-4}. Similar convergence level was obtained in the steady RANS simulations.

For the hybrid RANS/LES and LES model simulations the computational grids have been refined in the shear layer of the jet and in the near-wall regions as shown in Fig. 2. For the hybrid RANS/LES and RANS model computations the maximum value of y^{+} was less than 1

at the impingement plate, and less than 3 at the confinement plate. In LES, $y^+<3$ at all walls. The numbers of grid points are summarized in Table 1. The hybrid model simulations have been performed on the grids denoted by 'H/B=9.2, Re=20000', 'H/B=4, Re=18000' and 'H/B=2, Re=10000 (basic)' in Table 1. The LES model simulation has been performed on the finest grid, consisting of 15.1 million (M) grid points. The RANS simulations have been performed on 2D grids which are cuts in the x-y plane of the 3D grids used for the hybrid RANS/LES model simulations. We refer to our previous work [28] for a discussion of the grid independence in the simulations with the 2D RANS model.

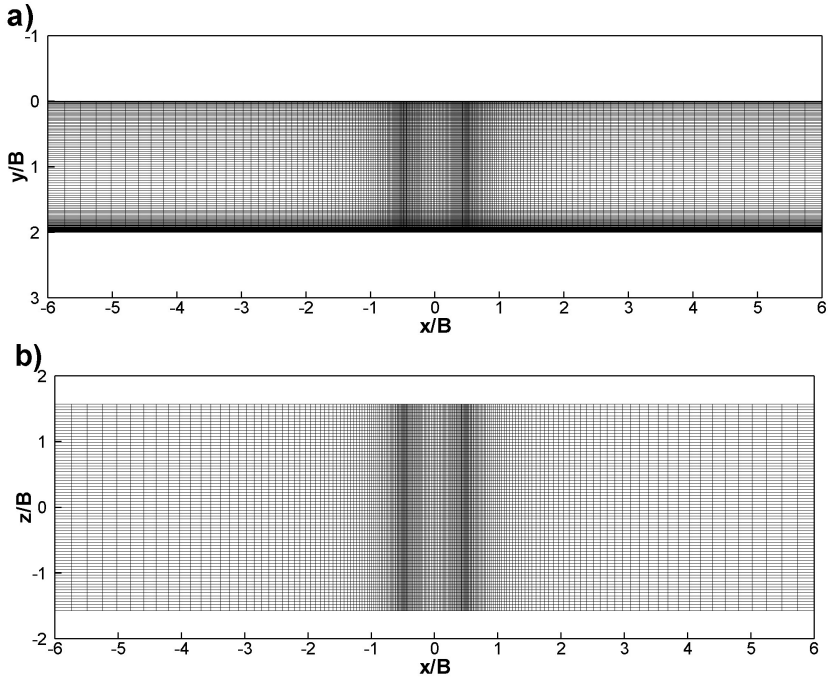

Figure 2. View of the computational mesh (a) in the x-y plane and (b) in the x-z plane (impingement plate) for simulation with the hybrid RANS/LES model (H/B=2).

4. Results

4.1. Inlet conditions

This section provides a verification of the two types of inlet conditions for simulation of the plane impinging jet with the hybrid RANS/LES model. The first way is using constant values of the turbulent kinetic energy, k, and the turbulent length scale, L_t, at the nozzle exit. The second way is using the exact shape of the inlet k-profile (as measured by Ashforth-Frost et al. [3]), together with a constant value of the turbulent (integral) length scale. The numerical results obtained with the hybrid RANS/LES model (impinging jet with the flat plate) are compared with the free jet flow measurements [4], so in absence of the impingement plate. Note the similar turbulent intensity level at the jet exit in the measurements by Zhe and Modi [4] and Ashforth-Frost et al. [3].

Panels a and b of Fig. 3 show the mean and fluctuating y-velocity components at distance y/H=0.3 from the nozzle exit for uniform profiles of the turbulent kinetic energy and the turbulent length scale over the inlet plane. The profiles have been averaged in time, in the spanwise z direction, and for positive and negative values of the x-coordinate with respect to the symmetry plane. It means that the numerical profiles have symmetry in Fig. 3 (also in Fig. 4, later). The computed mean velocity profile agrees well with the measured mean velocity

(Fig. 3 a). This justifies the selection of the exponent in Eq. (3.1). The predicted fluctuating velocity profile (Fig. 3 b) is in good agreement with measured fluctuating velocity over 60% of the jet width, but some underprediction of the peak values is observed.

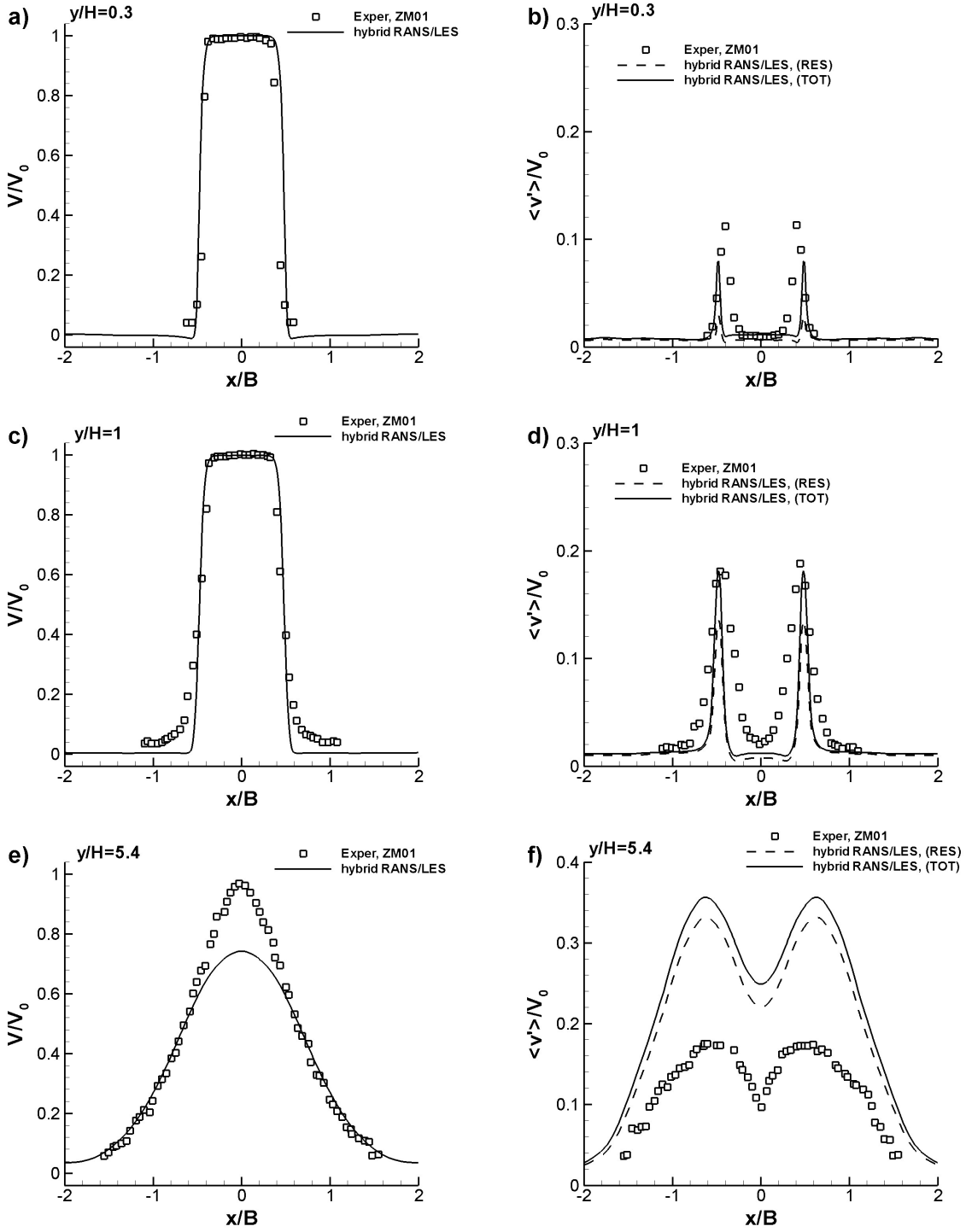

Figure 3. Profiles of mean y-velocity (a,c,e) and r.m.s. of fluctuating y-velocity component (b,d,f) for simulation of the plane impinging jet at H/B=9.2, Re=20000 at various distances from the jet exit: (a,b) y/H=0.3, (c,d) y/H=1, (e,f) y/H=5.4 and comparison with experiment (free jet). The resolved and total (resolved+modelled) velocity fluctuations are denoted by RES and TOT, respectively.

The peak values of v'/V_0 are better captured with the hybrid model further downstream at y/H=1 as shown in Fig. 3 (d), but the width of the turbulent shear layer is underestimated. The magnitude of the resolved fluctuating velocity at x/B=±0.5 is significantly higher at distance y/H=1 (Fig. 3 d) than immediately following the jet exit, y/H=0.3 (Fig. 3 b). This demonstrates that the hybrid model functions properly as the magnitude of the resolved scales gets higher with increasing distance from the jet exit, so when the width of the shear layer grows as a result of the Kelvin-Helmholtz instability. Further downstream (y/H=5.4), the jet spreads strongly (Fig. 3 e and f). In the simulations, the decay of the mean velocity is much stronger than in experiment. This is accompanied by an abrupt increase of the fluctuating velocity level (Fig. 3 f). The predicted mean and fluctuating velocity characteristics at distance y/H=5.4, so in the middle between the nozzle exit and the impingement plate, cannot be directly compared with the experimental results by Zhe and Modi [4] due to the effect of the impingement plate in the simulations. The impingement plate causes a strong flow recirculation inside the channel, leading to enhanced turbulent mixing in the jet flow region. Such flow recirculation is not present in the free jet flow. Overall, we observe good agreement between predicted and measured profiles of mean and fluctuating velocity at y/H=0.3 and 1 (Fig. 3 a-d), especially in the jet core region at y/H=0.3, which means that the inlet conditions have been set correctly.

Next, the effect of the inlet profiles of the turbulent kinetic energy is demonstrated in Fig. 4. Two ways of specifying the inlet conditions for the turbulent quantities are studied here. The first way consist of using uniform profiles of turbulent kinetic energy and turbulent length scale over the inlet plane (as done above), while the second way consists of using the exact shape of the inlet profile of the turbulent kinetic energy (reproduced from Ashforth-Frost et al. [3]), together with a constant value of the integral length scale. Improved results are obtained in the simulation with the hybrid model immediately downstream of the slot (y/H=0.3) using the exact shape of k-profile, but further downstream (y/H=1) a slightly too small width of the shear layers of the jet is still apparent. Fig. 4 demonstrates that for the case studied here (almost flat inlet mean velocity profile) the form of the inlet profile of k has only a secondary effect on the width of the turbulent shear layers downstream of the slot, provided the bulk values of the turbulent quantities are set correctly. This justifies the selection of uniform profiles of the turbulent quantities for the hybrid RANS/LES and LES model simulations discussed below.

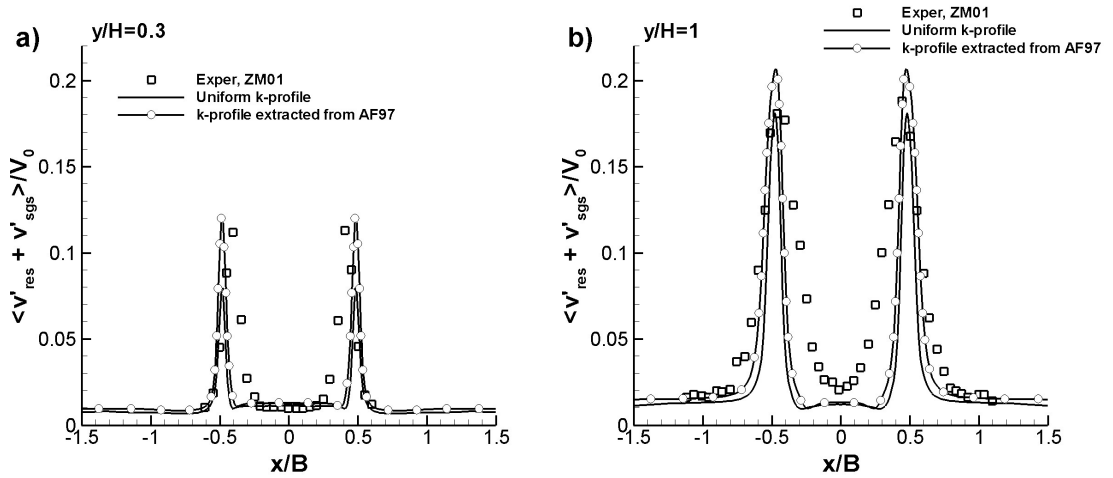

Figure 4. Profiles of fluctuating y-velocity component at distance y/H=0.3 (a) and y/H=1 (b) from the jet exit for simulation of the plane impinging jet at H/B=9.2, Re=20000 with uniform and variable inlet profile of turbulent kinetic energy.

4.2. Low Reynolds number case

This section gives an analysis of the numerical results obtained with the RANS, hybrid RANS/LES and LES models for simulation of the plane impinging jet at H/B=2 and Re=10000. The LES with the dynamic Smagorinsky model is performed on a very fine grid consisting of 15.1 M grid points. The LES results are used as reference data for comparison with the results obtained using the RANS and hybrid RANS/LES models. The numerical results are also compared with experimental data by Zhe and Modi [4].

Fig. 5 shows the mean streamwise velocity and fluctuating streamwise and wall-normal velocity components along the line perpendicular to the impingement plate at distance x/B=1 from the symmetry plane. For the hybrid and LES methods, the mean and fluctuating velocity data have been averaged in time and in the spanwise z direction.

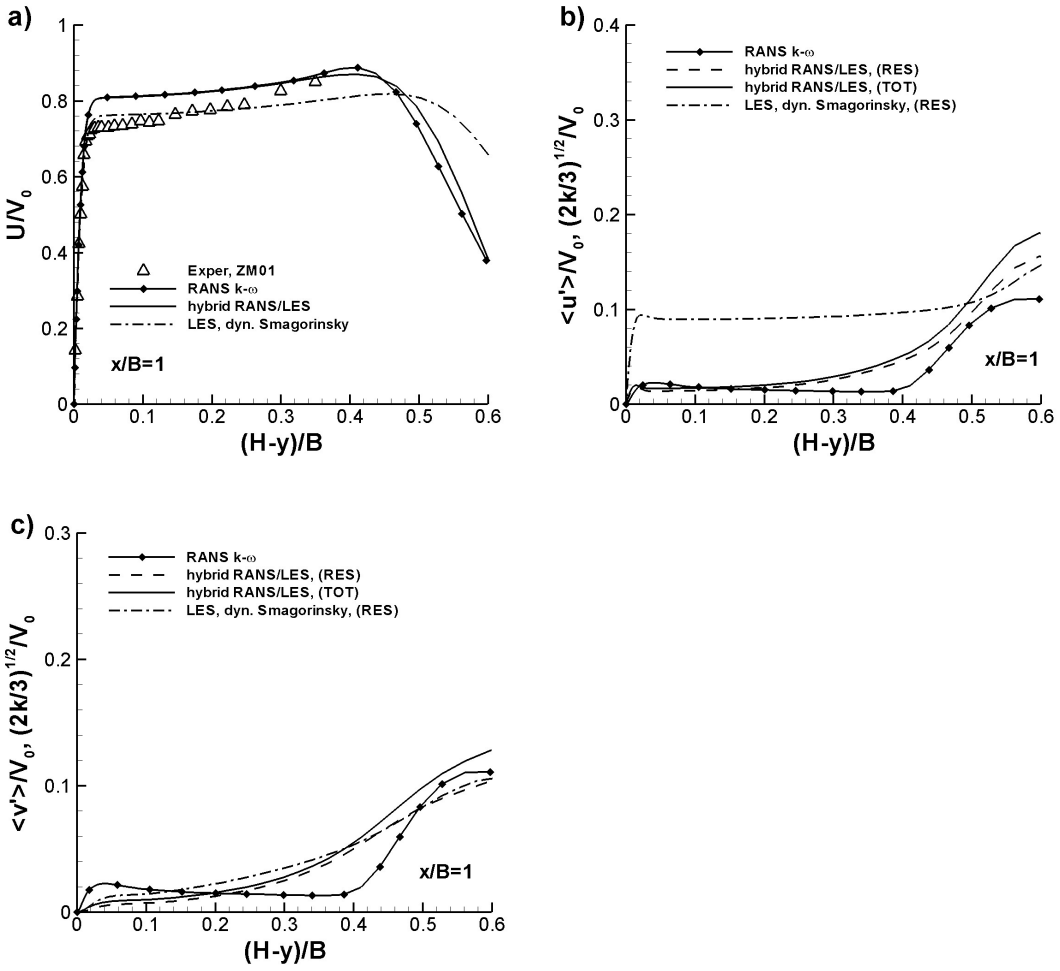

Figure 5. Profiles of mean streamwise velocity (a), streamwise fluctuating (b) and wall-normal (c) fluctuating velocity components for plane impinging jet simulation at H/D=2, Re=10000 at distance x/B=1 from the symmetry plane.

With RANS, the fluctuating velocities are computed by $u'=v'=(2k/3)^{1/2}$. Fig. 5 (a) shows that the mean velocity profiles obtained with the RANS and hybrid RANS/LES models are quite similar to the results of the LES and that they are in good agreement with the experiment. The LES results are in better agreement with the experimental data close to the wall owing to the fine grid applied there. Some differences between the different modelling techniques can be observed in Figs. 5 (b) and (c), showing the fluctuating velocity components. Note that in case

of the LES only the resolved fluctuations are shown. The hybrid RANS/LES model gives a much smaller level of the streamwise fluctuating component than LES, but very much comparable to that obtained with RANS. The wall-normal fluctuating velocity obtained with the hybrid model is close to the wall-normal fluctuating velocity reproduced using LES. A similar level of the fluctuating velocities is reproduced with all modelling techniques in the outer part of the developing wall jet, which shows that the flow dynamics is well captured in the shear layers of the jet for the small nozzle-plate distance discussed here.

Further downstream (Fig 6 a), some differences are visible on the mean velocity profiles predicted with RANS and computed with the hybrid RANS/LES and LES models. The close-up view of the near-wall region shows that RANS gives a too steep velocity gradient close to the wall, while the results of the hybrid RANS/LES model are in good agreement with the experimental data. The near-wall velocity gradient obtained with LES is slightly too small. The near-wall peak of the streamwise fluctuating velocity is well reproduced with the hybrid RANS/LES model (Fig. 6 b). LES reproduces a too high level of streamwise fluctuating component which leads to a too strong momentum reduction in the near-wall region (Fig. 6 a).

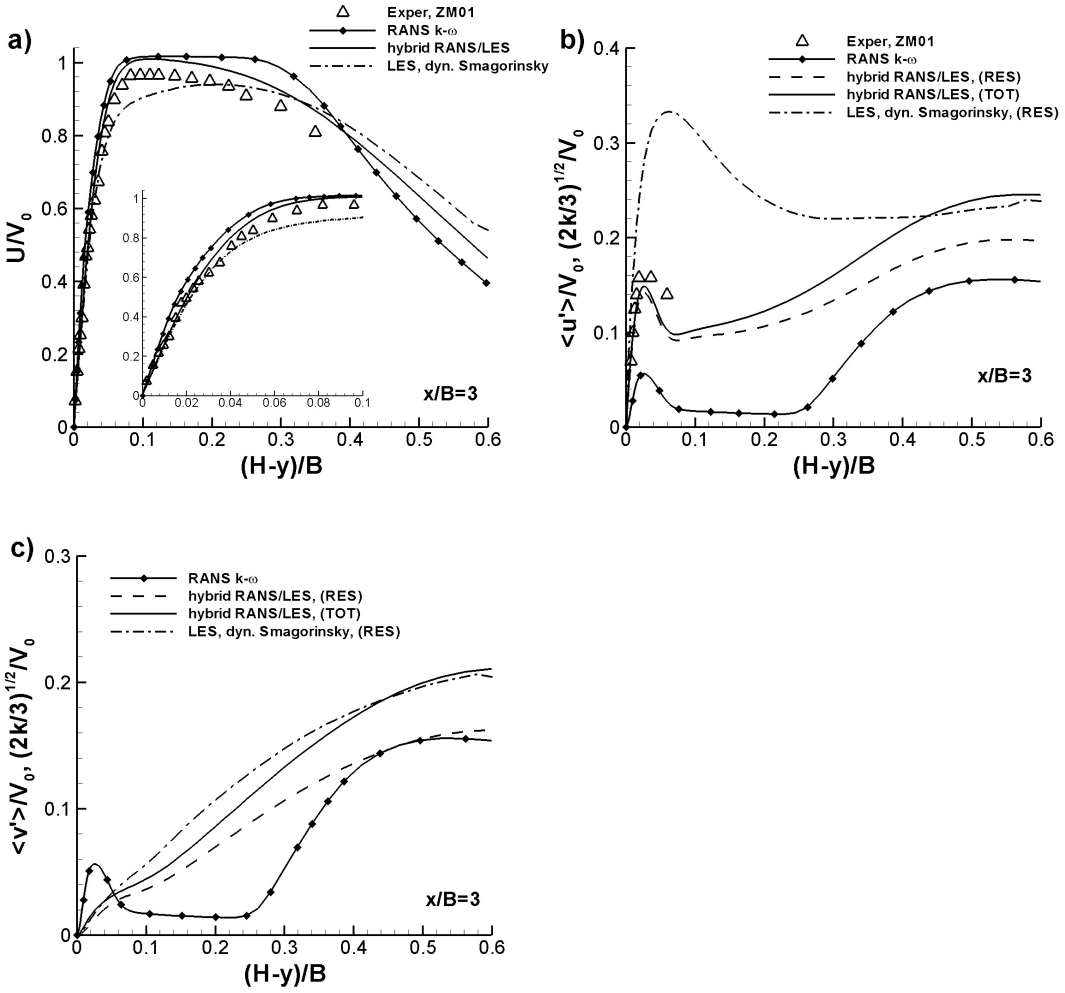

Figure 6. Profiles of mean streamwise velocity (a), streamwise fluctuating (b) and wall-normal (c) fluctuating velocity components for plane impinging jet simulation at H/B=2, Re=10000 at distance x/B=3 from the symmetry plane.

Fig. 7 shows the mean and fluctuating velocity profiles at x/B=5. Significant differences are observed here, between results obtained using the different modelling techniques. First of all, the distance x/B=5 seems to be already quite far from the symmetry plane for LES to be

reliable. Note again that the grid cells become more and more anisotropic (Fig. 2) with increasing distance from the symmetry plane. RANS overpredicts the peak value of the mean velocity, while the hybrid RANS/LES model seems to agree best with measurements by Zhe and Modi [4]. The overprediction of the fluctuating velocity components by LES can be explained by insufficient resolution to capture the final breakup phase of the vortex structures. It means that they are represented somewhat too large in the computation. This gives too large fluctuations. Similar conclusions were drawn by Chaouat and Schiestel [29] for LES of fully-developed turbulent channel flow. The LES technique of Chaouat and Schiestel was based on transport equations for the subgrid-scale stresses. The coarse grid LES results by Chaouat and Schiestel showed overprediction of the total streamwise stresses. The results improved on a finer grid. The overprediciton was explained by too large discretization errors (increased numerical diffusion) on a coarse grid which resulted in too large resolved structures. The results by Chaouat and Schiestel [29] support our observation that the grid has to be fine enough to capture the velocity characteristics along the impingement plate with the dynamic Smagorinsky model. The current simulation results show, however, less sensitivity to the grid density with the hybrid RANS/LES models than with the LES model. So, we have to accept that LES is reliable only in a limited zone of the developing wall-jet region, so for x/B<2.

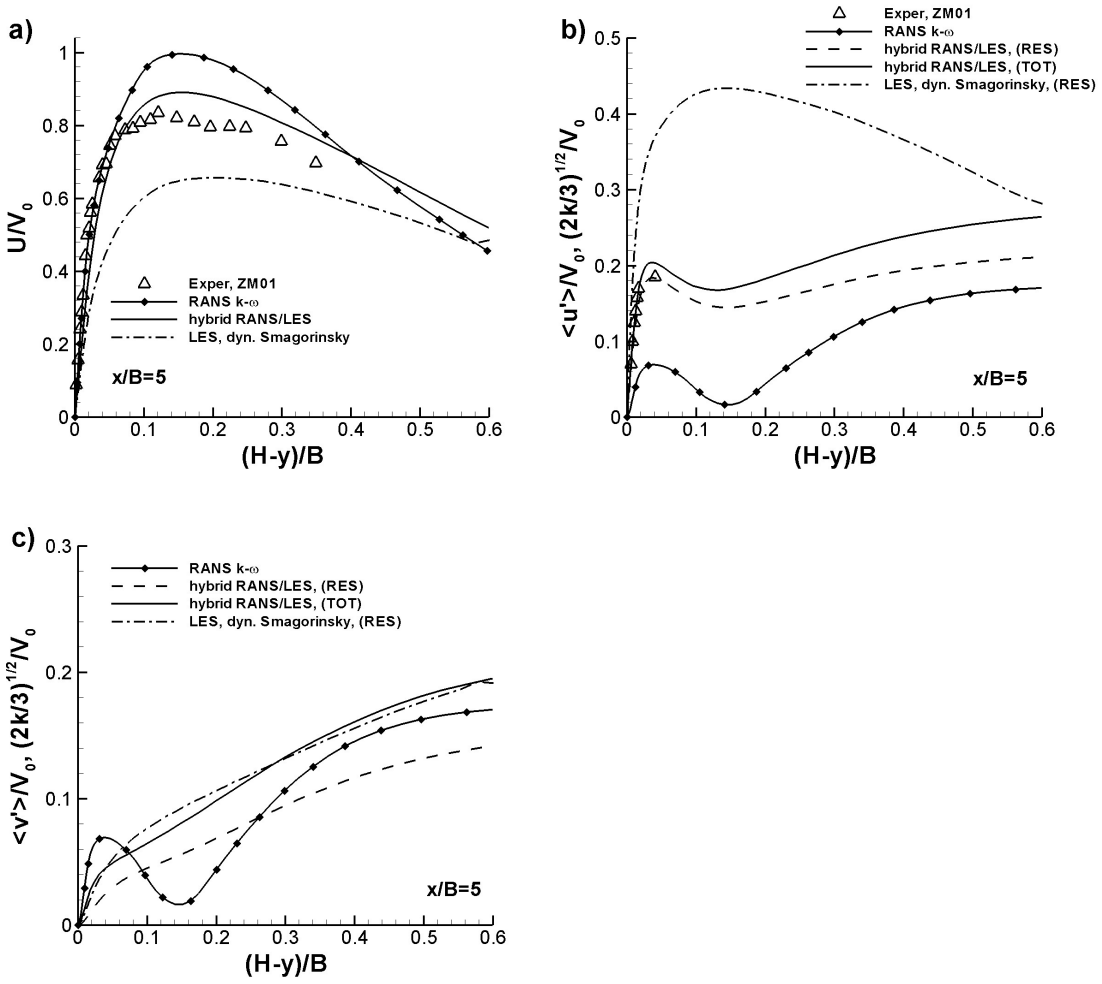

Figure 7. Profiles of mean streamwise velocity (a), streamwise fluctuating (b) and wall-normal (c) fluctuating velocity components for plane impinging jet simulation at H/B=2, Re=10000 at distance x/B=5 from the symmetry plane.

Contour plots of time-averaged mean and fluctuating velocities are presented in Figs. 8 and 9 in the x-y plane using RANS, hybrid RANS/LES and LES models. RANS shows the weakest spreading of the mean velocity profiles into the freestream among the three models tested. The differences between the hybrid and LES model results are clearly visible in Fig. 9 showing the fluctuating velocity component. The hybrid model reproduces a high level of turbulent fluctuations in the deflected shear layer of the jet. This seems to be realistic since, as discussed earlier, the mean velocity profiles reproduced with the hybrid model correspond well with the measured velocity profiles (Figs. 6 a and 7 a). The enhanced turbulence mixing becomes apparent in the near-wall region of the developing wall jet in Fig. 9 (b) from distance x/B=2 on. Again this is in good agreement with the experimental data shown in Figs. 6 (b) and 7 (b). LES is not able to capture the final phase of the vortex breakdown process in the near-wall region (Fig. 9 c), which results in a too high level of fluctuating velocity components at x/B>3, for the reasons explained above.

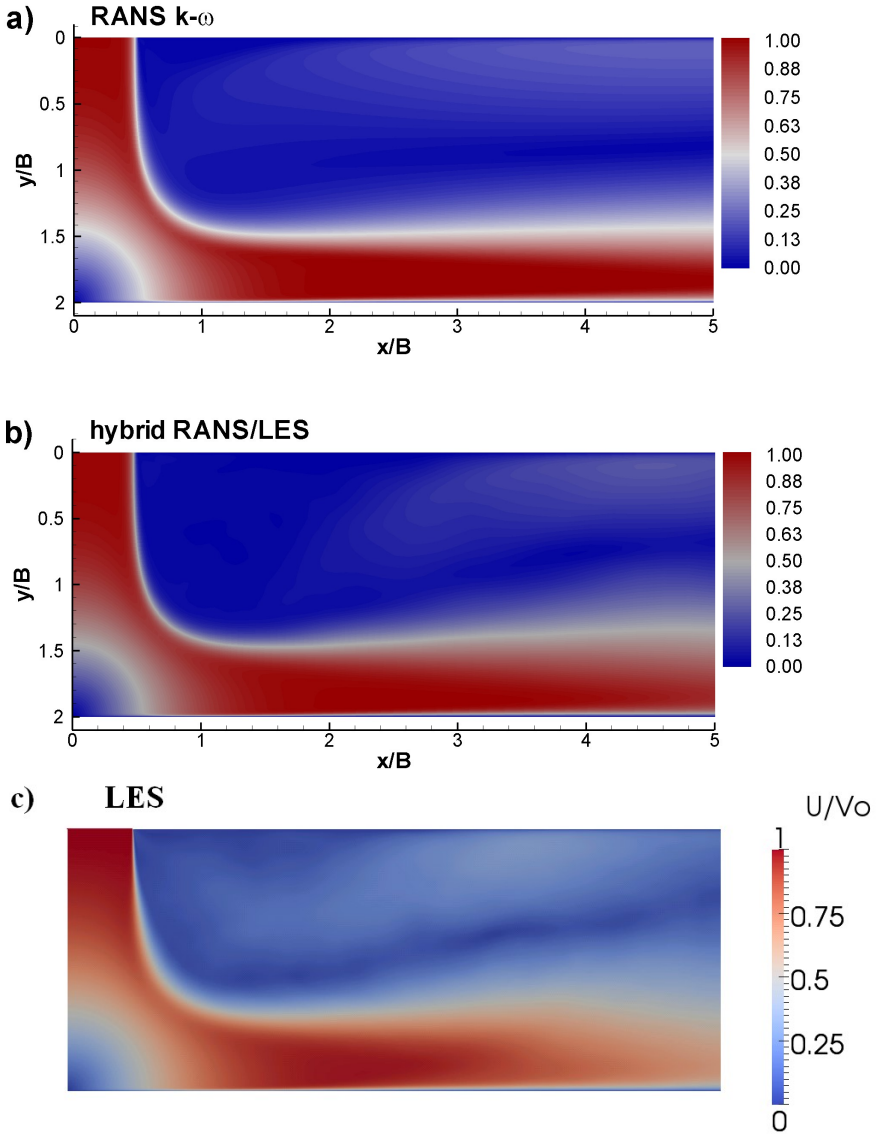

Figure 8. Contour plots of time-averaged velocity magnitude $|U|/V_0$ in the x-y plane for H/B=2, Re=10000 with a) the RANS k-ω, b) the hybrid RANS/LES (2.5 M cells) and c) the LES (15.1 M cells) models

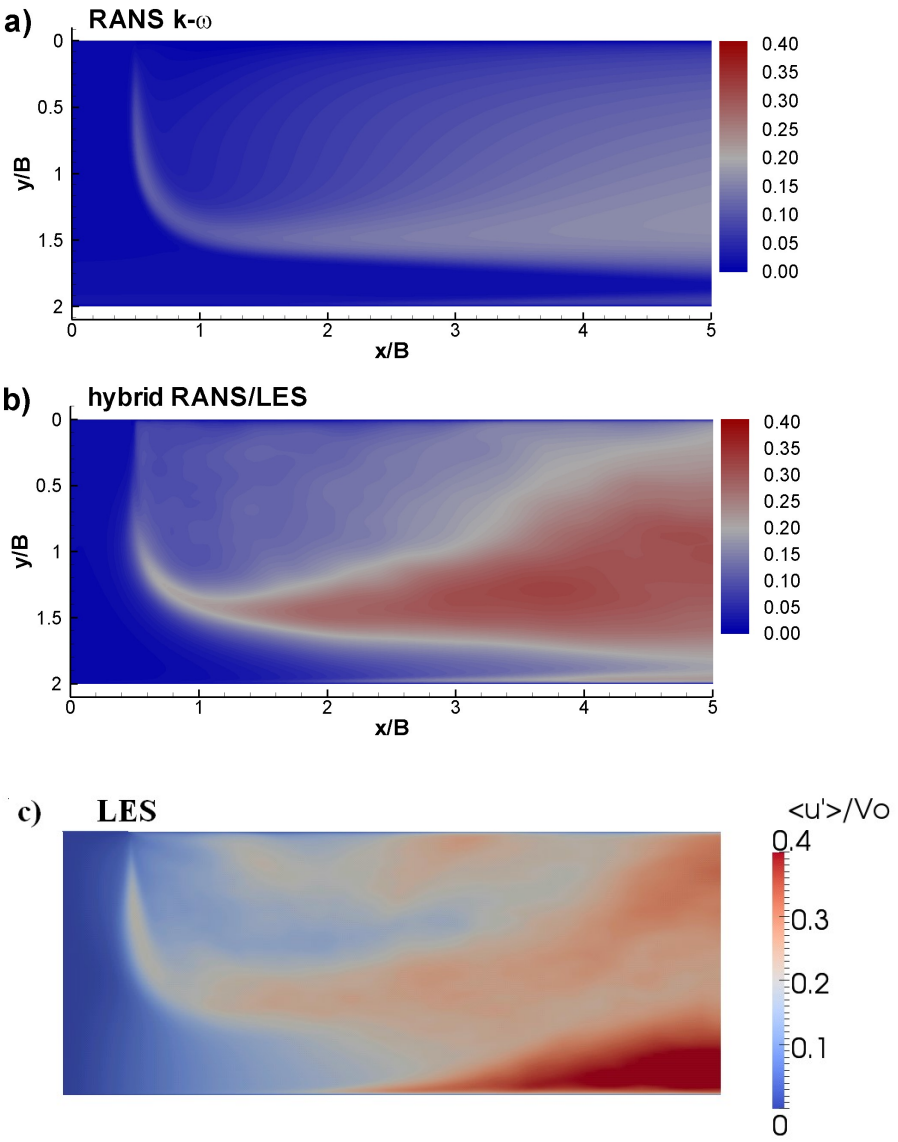

Figure 9. Contour plots of time-averaged r.m.s. of fluctuating velocity component $<u`>/V_0$ in the x-y plane obtained with a) the RANS k-ω, b) the hybrid RANS/LES (2.5 M cells) and c) the LES (15.1 M cells) models. In case of the hybrid and LES models the resolved fluctuations are shown. In RANS the fluctuating velocity means $(2k/3)^{1/2}/V_0$.

The profile of the skin friction coefficient is displayed in Fig. 10. The peak values obtained using RANS and the hybrid model are very similar to the peak value obtained using LES. RANS overpredicts the skin friction coefficient in the developing wall jet region (x/B>2), owing to a too high momentum near the wall, as shown in Fig. 6 (a) and Fig. 7 (a). For x/B>2, the skin friction profile reproduced with the hybrid RANS/LES model falls in between the skin friction profile obtained using RANS and LES. Again, we have to accept that the skin friction profile produced by LES is somewhat too low at distance x/B>2 due to lack of the grid resolution. Based on Fig. 6 (a) and Fig. 7 (a), which show that the velocity gradient near the wall obtained by the hybrid model compares very well with the experiments, we can conclude that the skin friction produced by the hybrid model is basically correct (we do not have explicitly the skin friction from the experiments).

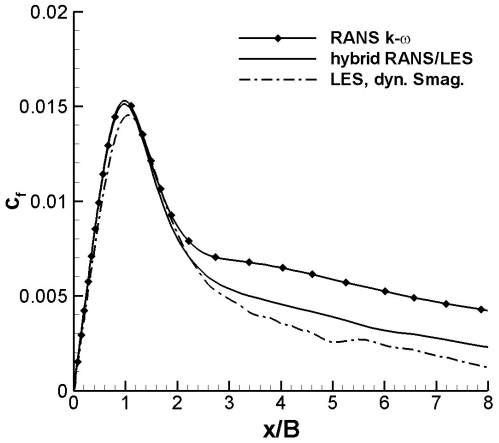

Figure 10. Skin friction coefficient for H/B=2, Re=10000.

The correspondence between the hybrid RANS/LES and LES model results is further analysed in Fig. 11 showing the contour plots of the Q-criterion ($Q=1/2(\Omega_{ij}\Omega_{ij} - S_{ij}S_{ij})$) in the x-z plane (horizontal plane) at distance (H-y)/B=0.02 from the impingement plate, obtained with the LES and the hybrid RANS/LES models. Both the LES and hybrid RANS/LES models reproduce the formation of spanwise-oriented vortex structures in the near-wall region of the developing wall jet at $1<|x/B|<3$. At first sight, the small-scale dynamics seems to be better captured with LES than with the hybrid model at $|x/B|>3$. This is due to higher grid resolution in the spanwise z direction which allows formation of smaller structures in case of the LES model (Table 1). The distance (H-y)/B=0.02 is very close to the wall, so most of the near-wall turbulence resides in RANS mode there in the hybrid model. More specifically, it means that the ratios of the modelled to the RANS eddy viscosity, ν_t/ν_{RANS} (where $\nu_{RANS}=k/\omega$) and the LES length scale to the turbulent length scale, $\min(C_{DES}\Delta/L_t,1)$, are equal to unity (results not shown here) over the complete x-z plane (Fig. 11). As a result, the modelled turbulence is somewhat larger with the hybrid model than with LES in the near-wall region of the developing wall-jet (Fig. 12), which compensates for the reduced activity of the small, resolved LES-like structures using the hybrid model. A verification of the fluctuating velocity components in Fig 6 (b) and Fig. 7 (b) allows to conclude that LES gives a wealth of the streamwise-oriented structures in Fig. 11 (a) at distance $|x/B|>3$ which are reproduced somewhat a too big. As mentioned, this is due to a grid coarsening with increasing distance from the symmetry plane.

Closer look to Fig. 12 (b) reveals weak streamwise oriented structures reproduced with the hybrid model at distance $|x/B|<1$. These structures appear as an effect of angular momentum instability in the flow region characterized by convex streamline curvature. Note that Tu and Wood (1996) speculated that these structures largely determine the level of the wall shear stress in the stagnation flow region for jet impingement at both high (H/B=12) and small nozzle-plate distances (H/B=4). These structures are not visible in the present LES results (Fig. 12 a). It is likely that somewhat a too high level of background fluctuations, which is reproduced in the stagnation flow region with LES (see Fig. 5 b) causes suppression of these streamwise oriented roll cells.

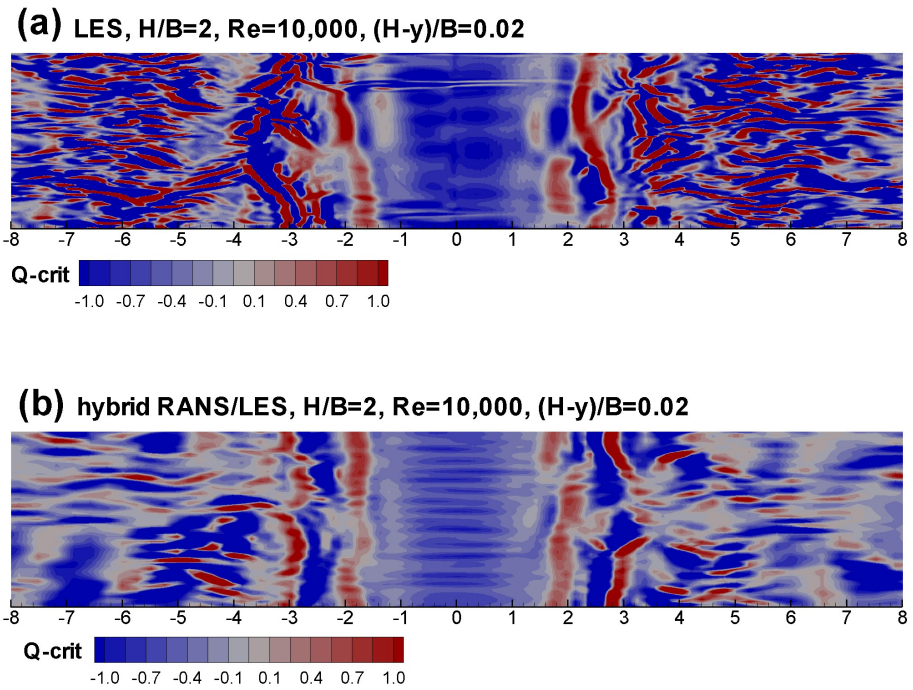

Figure 11. Contour plots of Q-criterion in the x-z plane at distance (H-y)/B=0.02 from the impingement plate obtained with (a) LES (15.1M cells) and (b) hybrid RANS/LES model (2.5M cells).

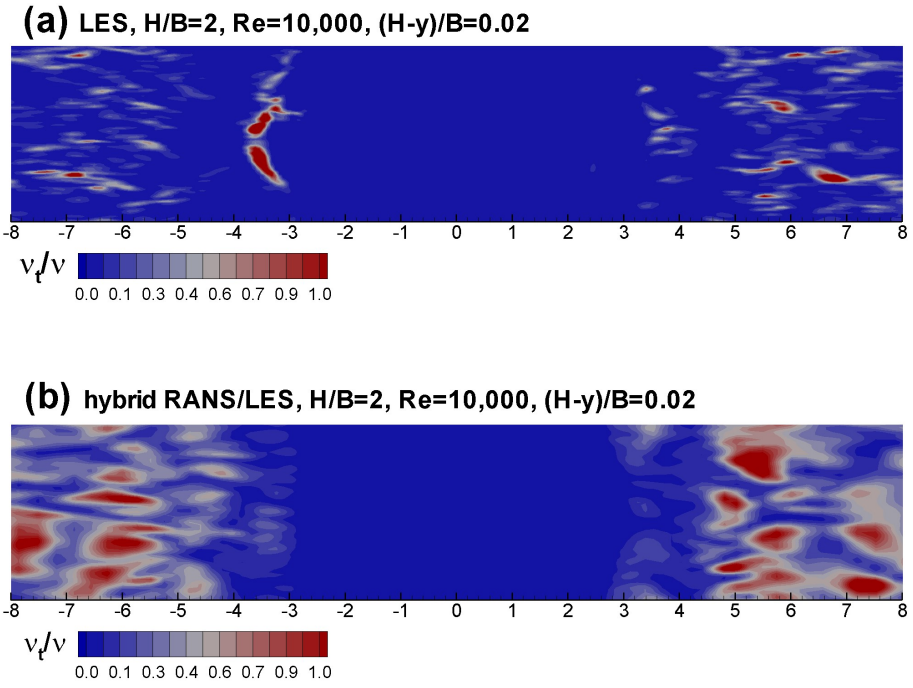

Figure 12. Contour plots of ratio of modelled to molecular viscosity in the x-z plane at distance (H-y)/B=0.02 from the impingement plate obtained with (a) LES (15.1M cells) and (b) hybrid RANS/LES model (2.5M cells).

4.3. High Reynolds number case

The present section discusses the mean and fluctuating velocity characteristics in the near-wall region of the developing wall jet for simulation of the plane impinging jet at H/B=4, Re=18000 with the k-ω RANS and the hybrid RANS/LES models. The numerical results are compared with experimental data by Zhe and Modi [4], Ashforth-Frost et al. [3] and Dogruoz [7]. As shown in Fig. 13 (a, c) and (e) the streamwise velocity profiles reproduced with the k-ω RANS model are in good agreement with measured velocity profiles except very near to the wall where RANS gives a too steep velocity gradient.

The near-wall behaviour is better captured with the hybrid RANS/LES model. This is demonstrated in the close-up view of the near-wall region shown in Fig. 13 (c). Panels b, d and f of Fig. 13 show the comparison between numerical and measured fluctuating streamwise velocity components. The measured wall-normal fluctuating components are not available for this test case, but from Fig 13 (b) we can speculate that RANS slightly overpredicts the turbulent kinetic energy in the impact zone. The hybrid RANS/LES model gives a too high streamwise fluctuating velocity at y/B=1 (Fig. 13 b), but the near-wall fluctuating velocity is much better captured with the hybrid model further away from the symmetry plane (Fig. 13 d and f). The hybrid model has a tendency to reproduce a too high level of fluctuating velocity away from the wall ((H-y)/B>0.2). This might be an indication that the vortex structures produced by the hybrid model are too large there.

Fig. 14 shows the skin friction coefficient along the impingement plate for H/B=4, Re=18000. The numerical results are compared with experimental data by Dogruoz [7]. RANS is in error in the transition zone (2<x/B<7). With the hybrid model, the deficiency is cured.

Summing up, the hybrid RANS/LES model gives realistic mean and fluctuating velocity profiles along the impingement plate at H/B=4, Re=18000. The RANS model has the tendency to overpredict the mean velocity gradient in the near-wall region of the developing wall jet. The dip in the skin friction profile is not captured using RANS despite the stress-limiter (Eq. 2.5). It means that the stress-limiter is not sufficiently strong in the developing wall jet region. The flow details in the transition from the stagnation flow to the developed wall jet region are much better reproduced with the hybrid RANS/LES model than using RANS.

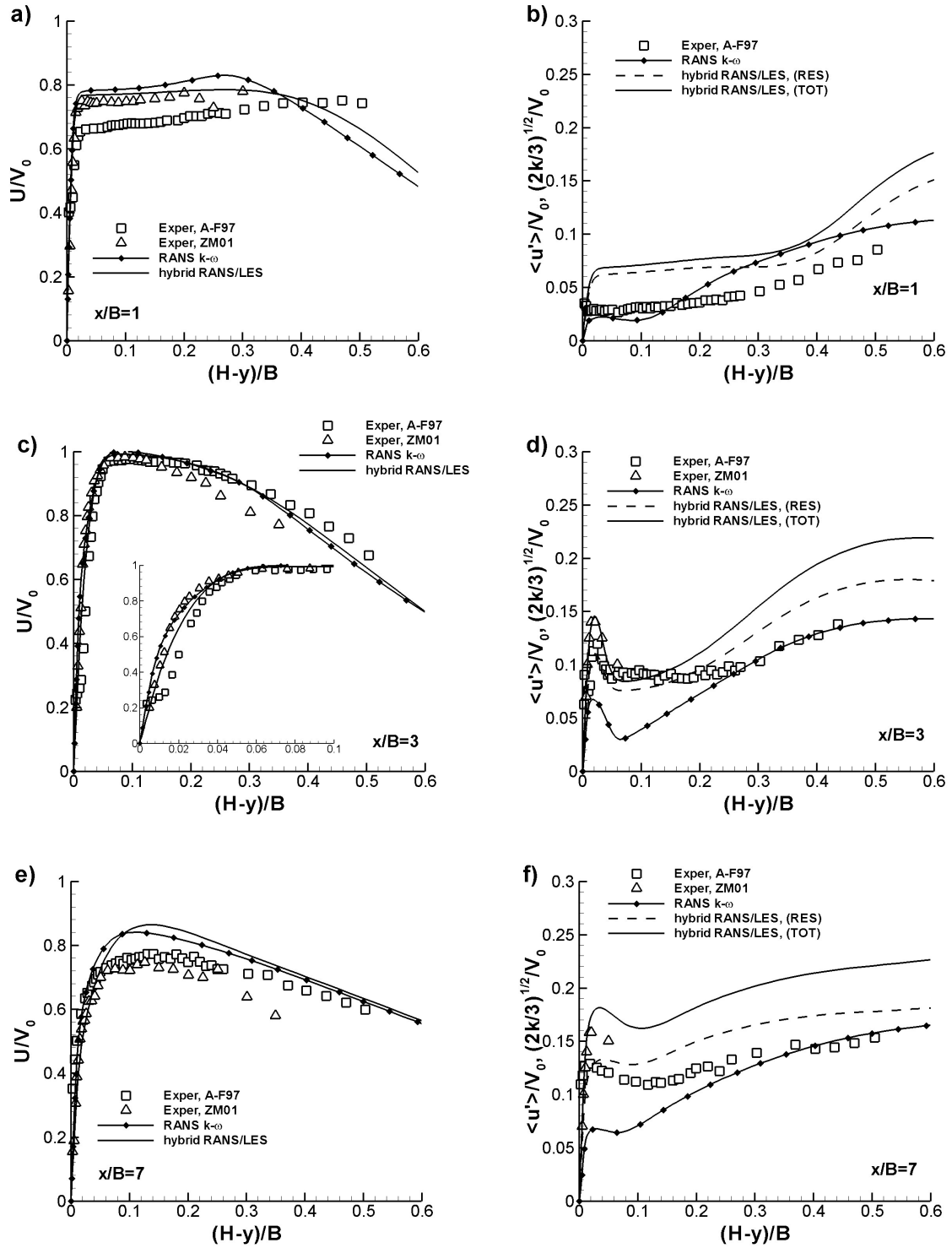

Figure 13. Profiles of mean streamwise velocity (a,c,e) and r.m.s. of streamwise fluctuating velocity component (b,d,f) for simulation of the plane impinging jet at H/D=4, Re=18000 at various distances from the symmetry plane: (a,b) x/B=1, (c,d) x/B=3 and (e,f) x/B=7. In case of the hybrid model the resolved and total (resolved+modelled) fluctuations are denoted by RES and TOT, respectively.

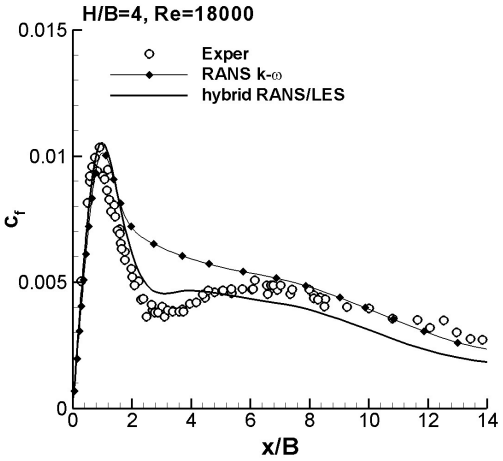

Figure 14. Skin friction coefficient for H/B=4, Re=18000

5. Summary

The results of simulations of plane impinging jets at different nozzle-plate distances (H/B=2, 4 and 9.2) and three Reynolds numbers (Re=10000, 18000, 20000) using a k-ω based hybrid RANS/LES model were presented. The k-ω RANS model has been employed for the low nozzle-plate distance cases (H/B=2 and 4). Reference results using LES with the dynamic Smagorinsky model were generated for H/B=2, Re=10000.

Overall, good agreement with the experimental data of Zhe and Modi [4] has been obtained with the hybrid RANS/LES model for jet impingement at H/B=4 and Re=18000 in terms of the mean and fluctuating velocity profiles along the plate. Very good agreement between computed and measured skin friction coefficient along the impingement plate has been obtained with the hybrid RANS/LES model for H/B=4, Re=18000. The hybrid model results agree also well with the reference LES results in the stagnation flow region (x/B<2) for H/B=2, Re=10000. With the RANS model, the stress-limiter is not strong enough, leading to a too large wall shear stress reproduced with RANS along the impingement plate.

Acknowledgements

The first author acknowledges an international cooperation grant of Ghent University and the support from a research project funded by the Polish National Science Centre (decision number DEC-2011/01/B/ST8/07267).

References

[1] C.V. Tu, D.H. Wood, *Wall pressure and shear stress measurements beneath an impinging jet*, Experimental Thermal and Fluid Sci., **13**, 364-373, 1996.

[2] J. Sakakibara, K. Hishida, M. Maeda, *Vortex structure and heat transfer in the stagnation region of an impinging plane jet (simultaneous measurements of velocity and temperature fields by digital particle image velocimetry and laser-induced fluorescence),* Int. J. Heat Mass Transfer, **40**, 3163-3176, 1997.

[3] S. Ashforth-Frost, K. Jambunathan, C.F. Whitney, *Velocity and turbulence characteristics of a semiconfined orthogonally impinging slot jet*, Experimental Thermal and Fluid Science, **14**, 60-67, 1997.

[4] J. Zhe, V. Modi, *Near wall measurements for a turbulent impinging slot jet*, Trans. of the ASME, J. Fluid Eng., **123**, 112-120, 2001.

[5] Y. Guo, D.H. Wood, *Measurements in the vicinity of a stagnation point*, Experimental Thermal and Fluid Science, **25**, 605–614, 2002.

[6] V. Narayanan, J. Seyed-Yagoobi, R.H. Page, *An experimental study of fluid mechanics and heat transfer in an impinging slot jet flow*, Int. J. Heat and Mass Transfer, **47**, 1827–1845, 2004.

[7] M.B. Dogruoz, *Experimental and Numerical Investigation of Turbulent Heat Transfer due to Rectangular Impinging Jets*, Ph.D. Thesis, The University of Arizona, Tucson, Arizona, 2005.

[8] J. Senter, C. Solliec, *Flow field analysis of a turbulent slot air jet impinging on a moving flat surface*, Int. J. Heat Fluid Flow, **28**, 708-719, 2007.

[9] T. Cziesla, G. Biswas, H. Chattopadhyay, N.K. Mitra, *Large-eddy simulation of flow and heat transfer in an impinging slot jet*, Int. J. Heat Mass Transfer, **22**, 500-508, 2001.

[10] F. Beaubert, S. Viazzo, *Large eddy simulations of plane turbulent impinging jets at moderate Reynolds numbers*, Int. J. Heat Fluid Flow, **24**, 512-519, 2003.

[11] M. Tsubokura, T. Kobayashi, N. Taniguchi, W.P. Jones, *A numerical study on the eddy structures of impinging jets exited at the inlet*, Int. J. Heat Fluid Flow, **24**, 500-511, 2003.

[12] H. Hattori, Y. Nagano, *Direct numerical simulation of turbulent heat transfer in plane impinging jet*, Int. J. Heat Fluid Flow, **25**, 749-758, 2004.

[13] J.A. Fernandez, J.C. Elicer-Cortes, A. Valencia, M. Pavageau, S. Gupta, *Comparison of low-cost two-equation turbulence models for prediction flow dynamics in twin-jets devices*, Int. Commun. Heat Mass Transfer, **34**, 570-578, 2007.

[14] J.E. Jaramillo, C.D. Perez-Segarra, I. Rodriguez, A. Oliva, *Numerical study of plane and round impinging jets using RANS models*, Numer. Heat Transfer Part B, **54**, 213-237, 2008.

[15] D.C. Wilcox, *Formulation of the k-ω turbulence model revisited*, AIAA Journal, **46**, 2823-2837, 2008.

[16] M. Strelets, *Detached eddy simulation of massively separated flows*, AIAA Paper 2001-0879, 2001.

[17] J. Fröhlich, D. von Terzi, *Hybrid LES/RANS methods for the simulation of turbulent flows*, Progress in Aerospace Sciences, **44**, 349–377, 2008.

[18] L. Davidson, S.H. Peng, *Hybrid LES-RANS modelling: a one-equation SGS model combined with a k-ω model for predicting recirculating flows*, Int. J. Numer. Meth. Fluids, **43**, 1003-1018, 2003.

[19] J.C. Kok, H. Dol, H. Oskam, H. van der Ven, *Extra-large eddy simulation of massively separated flows*, AIAA Paper 2004-0264, 2004.

[20] J. Yan, C. Mocket, F. Thiele, *Investigation of alternative length scale substitutions in detached-eddy simulation*, Flow Turbulence and Combustion, **74**, 85-102, 2005.

[21] S. Kubacki, E. Dick, *Hybrid RANS/LES of flow and heat transfer in round impinging jets*, Int. J. Heat Fluid Flow, **32**, 631-651, 2011.

[22] S. Kubacki, E. Dick, *Simulation of plane impinging jets with k-ω based hybrid RANS/LES models*, Int. J. Heat Fluid Flow, **31**, 862-878, 2010.

[23] S. Kubacki, J. Rokicki, E. Dick, *Hybrid RANS/LES computation of plane impinging jet flow*, Arch. Mech., **63**, 117-136, 2011.

[24] A. Scotti, C. Meneveau, D.K. Lilly, *Generalized Smagorinsky model for anisotropic grids*, Phys. Fluids A, **5**, 2306–2308, 1993.

[25] P.R. Spalart, S. Deck, M.L. Shur, K.D. Squires, M. Strelets, A. Travin, *A new version of detached-eddy simulation, resistant to ambiguous grid densities*, Theor. Comput. Fluid Dyn., **20**, 181-195, 2006.

[26] D.C. Wilcox, Turbulence Modeling for CFD. Second edition, DCW Industries Inc., La Canada CA, 1998.

[27] F. Mathey, D. Cokljat, J.P. Bertoglio, E. Sergent, *Assessment of the vortex method for Large Eddy Simulation inlet conditions*, Progress Comput. Fluid Dynamics, **6**, 58-67, 2006.

[28] S. Kubacki, E. Dick, *Convective heat transfer prediction for an axisymmetric jet impinging onto a flat plate with an improved k-ω model*, Int. J. Numer. Methods in Heat and Fluid Flow, **19**, 960-981, 2009.

[29] B. Chaouat, R. Schiestel, *A new partially integrated transport model for subgrid-scale stresses and dissipation rate for turbulent developing flows*, Phys. Fluids, **17**, 065106, 2005.